International Journal of Materials Science and Technology Studies
ISSN: 3006-7693 (Print), ISSN: 3006-3744 (Online) | Volume 5, Number 1, Year 2026
DOI: https://doi.org/10.62051/ijmsts.v5n1.06
Journal homepage: https://wepub.org/index.php/IJMSTS/index

Study on Welding Properties of QP1500

Kejia Qiang

University of Shanghai for Science and Technology, Shanghai, China

ABSTRACT

With the increasing demand for lightweight and high-strength and toughness materials in the automotive, construction machinery, and other fields, quenched and partitioned (Q&P) steel has become a research hotspot due to its excellent strength-ductility matching characteristics [1]. QP1500 high-strength quenched and partitioned steel undergoes welding processing in engineering applications, and the welding method significantly affects its microstructural stability and resistance to hydrogen embrittlement, which is crucial for the safety of component service [2]. This study takes QP1500 steel as the object to explore its microstructure and mechanical properties, focusing on analyzing the regulation of microstructural evolution and hydrogen embrittlement sensitivity by tailor welding and L-bend welding [3]. By combining microscopic analysis methods such as optical microscopy (OM) and scanning electron microscopy (SEM) with tensile testing, slow strain rate testing (SSRT), and hydrogen permeation testing, the process-microstructure-property correlation is revealed. The results show that high power promotes martensitic grain refinement, enhancing tensile strength and elongation. The hardness of the welding start, middle, and end surfaces exhibits the same trend. The end surface hardness is relatively high, showing a gradual upward trend. The hardness of the welding start surface is the lowest. This study provides theoretical and technical support for the optimization of engineering welding processes and hydrogen embrittlement resistance design of QP1500 steel, which is of great significance for promoting the industrial application of high-strength Q&P steel [4].

KEYWORDS

Laser welding; Lap welding; QP steel; Hydrogen embrittlement

1. QP1500 MICROSTRUCTURE OF BASE METAL

The microstructure of qp1500 steel base metal was analyzed by optical microscope (OM) and scanning electron microscope (SEM). The results are shown in Figure1:

Content from this work may be used under the terms of CC BY-NC 4.0 licence (https://creativecommons.org/licenses/by-nc/4.0/).
Published by Warwick Evans Publishing.

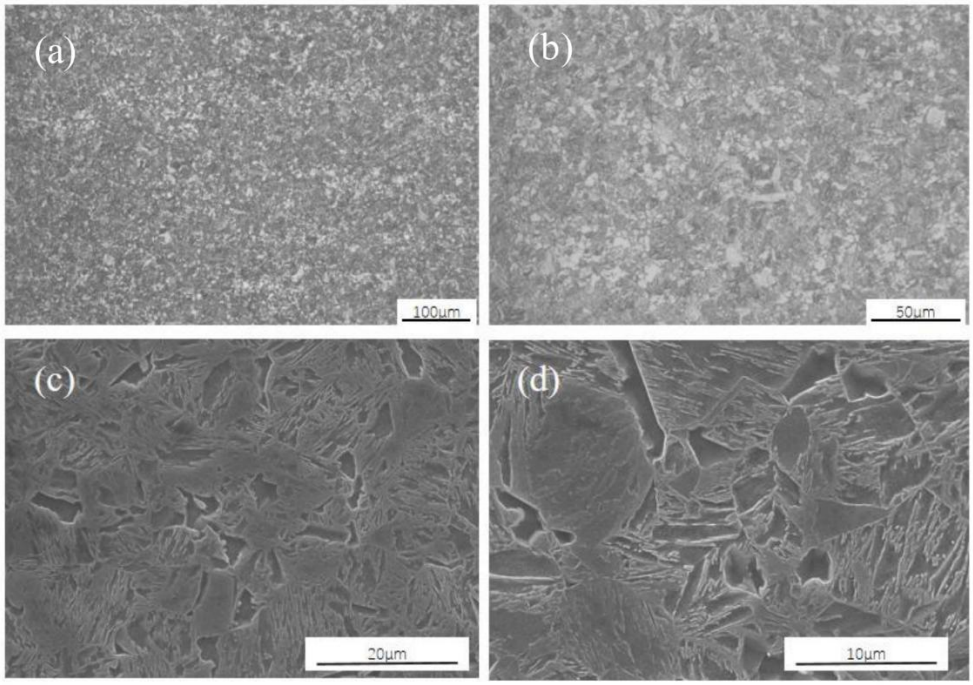

Figure 1. qp1470 microstructure (a) - (b) metallography; (c) - (d) scan

Figure 1 (a) - (b) shows the metallographic diagram of qp1500 steel microstructure, and figure 1 (c) - (d) shows the scanning diagram of qp1500 steel microstructure under different magnification. The microstructure of qp1500 is composed of dark ferrite grains, gray martensite islands and retained austenite. The base metal of dual phase steel usually has high strength and good toughness, which is the result of the joint action of ferrite, martensite and retained austenite.

2. QP1500 BUTT WELDING

2.1. Butt Welding Process

QP1500 steel is welded by five different welding processes. The welding processes are as follows:

Table 1. qp1500 welding process

Parameter / Number	Laser power/kW	Speed/m·min^{-1}	Defocus/mm	Shielding gas/L·min^{-1}
1	2.5	4	-2	20
2	3	4	-2	20
3	3.5	4	-2	20
4	4	4	-2	20
5	3	4	-3	0
6	3	9	-3	15
8	3	10.2	-3	15

2.2. Mechanical Properties of Butt Welding

The tensile strength of the base metal is 1496.28 MPa and the elongation is 15.84%. Control the welding speed to 4m/min, -4mm defocus, and the argon protection of 20l/min remains unchanged. It can be seen from figure 30 that with the increase of welding power, the mechanical properties of qp1470 steel decreased first and then increased after welding. When the welding power increases to 4000W, the tensile strength of the sample is 1069.24 MPa, the elongation is 4.82%, and the mechanical properties are the best. When the welding power is 4000W, the laser energy distribution

tends to be uniform, the width of the molten pool decreases, and the cooling rate is moderate, which promotes the refinement of martensite grains and the formation of fine ferrite. Through the fine grain strengthening effect, the tensile strength and elongation are improved at the same time. At this time, the weld formation is good and there are fewer defects, achieving the best mechanical property matching.

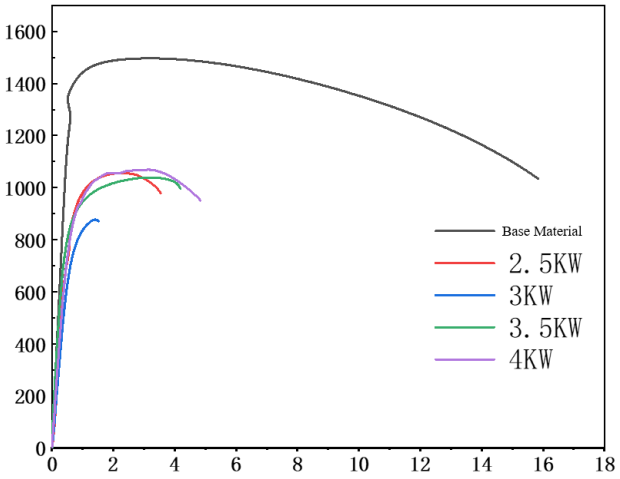

Figure 2. Stress strain curve under different welding power

2.3. Welding Microstructure

The macro morphology and microstructure of heat affected zone of qp1470 steel after laser welding were characterized by SEM, as shown in Fig. 3 (A-F).

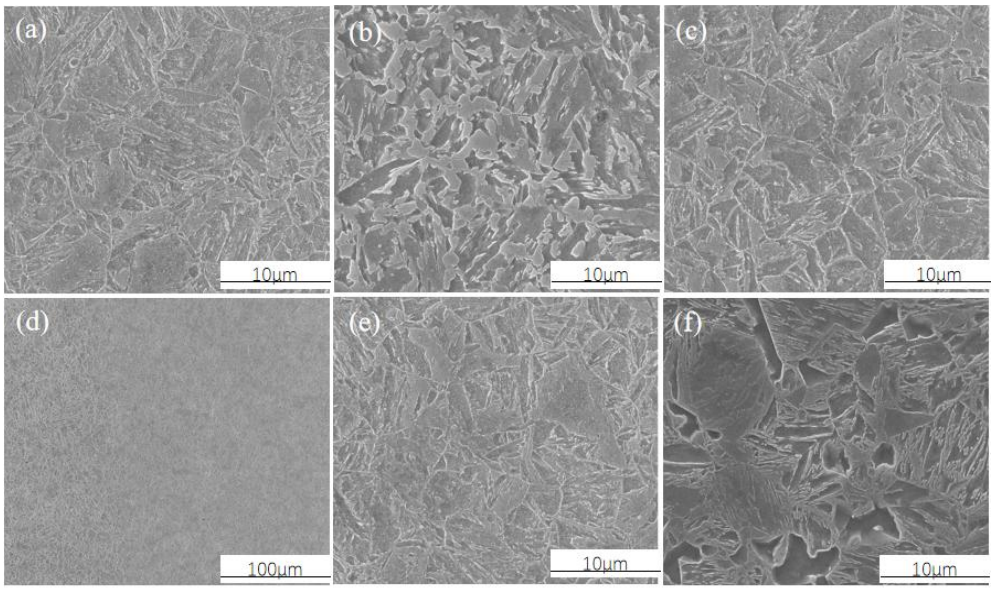

Figure 3. (a) weld zone; (b) Coarse grained region; (c) Fine grain region; (d) Critical heat affected zone; (e) Heat affected zone; (f) Base metal

Fig. 3 (A-F) is the scanning organization chart of 4000W, 4m/min, -4mm defocus, 20l/min argon shielded welding joint. In the process of laser welding, the distance between each area of the welded joint and the center of the welding heat source is different. This difference in distance leads to great differences in peak heating temperature, residence time and cooling rate in different regions. Therefore, under the scanning electron microscope, the microstructure of each region is also different. The microstructure of welded joints is generally divided into six different regions, as shown in Figure 3, which are weld zone, coarse grain zone, fine grain zone, critical heat affected zone, heat affected

zone and base metal zone. This area is basically composed of coarse lath martensite, mainly because the weld experienced rapid heating and rapid cooling during the welding process, making the austenite in the structure transformed into martensite. The SEM diagram of coarse-grained zone structure is shown in Fig. 3 (b). This zone is adjacent to the weld zone during welding, and there is no melting during heating, but the temperature at this time can reach above AC3. The original structure in the base metal is completely austenitized, and the heating temperature is relatively high, resulting in grain growth of the austenitic structure in this region, and then coarse lath martensite is generated during rapid cooling. Fig. 3 (c) is the SEM diagram of the microstructure of the fine-grained region. The lath martensite in the microstructure changes from coarse to fine, mainly because this region is far away from the weld zone than the coarse-grained region, the peak temperature is lower than the coarse-grained region, and higher than AC3, and its residence time at high temperature is shorter than that in the weld zone. The SEM diagram of the structure of the critical heat affected zone is shown in Figure 3 (d). During welding, the temperature in this zone is heated to between AC1 and AC3, and part of the ferrite and martensite structure are transformed into austenite structure. After rapid cooling, part of the austenite structure is transformed into martensite structure, while the microstructure without austenite transformation remains. Therefore, the structure in this zone is a mixed structure of lath martensite, massive ferrite and a small amount of residual austenite. Fig. 3 (E) shows the SEM image of the microstructure of the heat affected zone. Because the heating temperature in this zone is lower than AC1, there is no austenite transformation. Therefore, it can be seen from Fig. 3 (E) that carbide precipitates, which is caused by the decomposition of martensite. Finally, the structure of this region is composed of tempered martensite, massive ferrite and a small amount of retained austenite.

The samples of 3000W, 4m/min, -3mm, airless, 3000W, 10.2m/min, -3mm, 15l/min, 3000W, 9m/min, -3mm, 15l/min were welded by different processes through 20mm*150mm welding strip samples. Among them, 3000W, 9m/min, -3mm and 15l/min welding samples are relatively good in macro morphology. Figure 33 shows the metallographic structure of 3000W, 9m/min, -3mm and 15l/min. The fusion width is 1.3mm.

3. LASER L-BEND WELDING

3.1. Laser L-Bend Welding Process and Corresponding Penetration/Width

Table 2. laser L-Bend welding process and corresponding penetration/width

Parameter / Number	Laser power/kW	Speed /m·min^{-1}	Defocus /mm	Shielding gas /L·min^{-1}	Wielding depth / mm	Wielding width/ mm
L-1	2.5	4	-4	20	3.7	0.9
L-2	3	4	-4	20	2.3	1.2
L-3	3.5	4	-4	20	3.1	1.0
L-4	4	4	-4	20	3.5	1.1
L-5	3.5	4	-4	0	2.7	1.4
L-6 (Original surface)	4	4	-4	20	3.9	1.1
L-7 (Oiling)	4	4	-4	20	3.6	1.1

The penetration depth/width of the joint welded by laser under the protection of 4000W, 4m/min, -4mm defocus and 20l/min argon basically meets the requirements of 3.4mm/1mm.

3.2. Microstructure Characterization of Laser L-Bend Welded Joint

The metallographic structure of the joint meeting the technical requirements is shown in Figure 4:

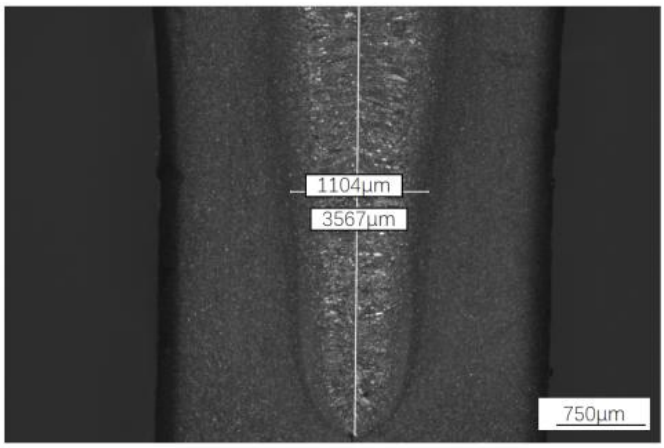

Figure 4. (a) 4000W 4m/min-4mm 20l/min

The penetration depth and width of welds meeting the requirements from the start point to the end point are relatively consistent, and the welding is relatively uniform. In addition, the parameters of 4000W, 4m/min, -4mm defocus and 20l/min argon shielded welding were used to weld the surface in a variety of states: the surface was not polished and the surface was coated with oil. Figure 5 (a) shows the metallographic structure of the welded surface in the ungrinded state, and Figure 5 (b) shows the metallographic structure of the welded surface in the oiled state. The penetration depth and width of the surface coated with oil are 1.1mm and 3.6mm respectively. The penetration depth and width of the surface not polished are 1.1mm and 3.9mm respectively, which meet the requirements.

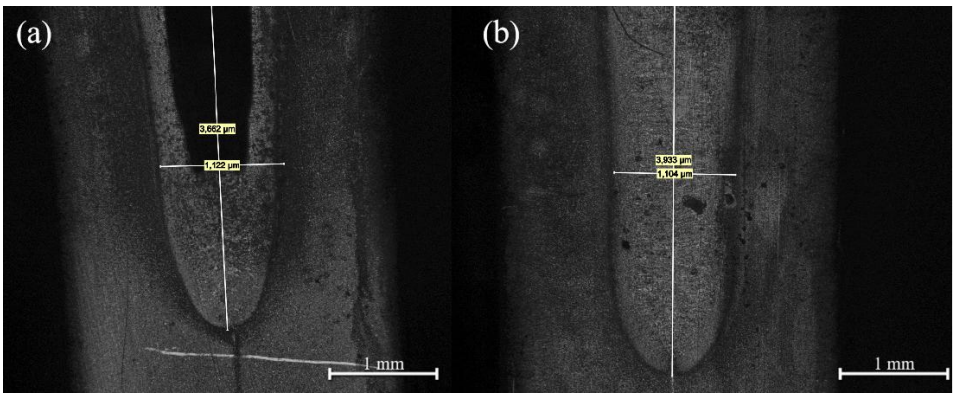

Figure 5. (a) surface oiling state; (b) Surface not polished

3.3. Properties of Laser L-Bend Welded Joint

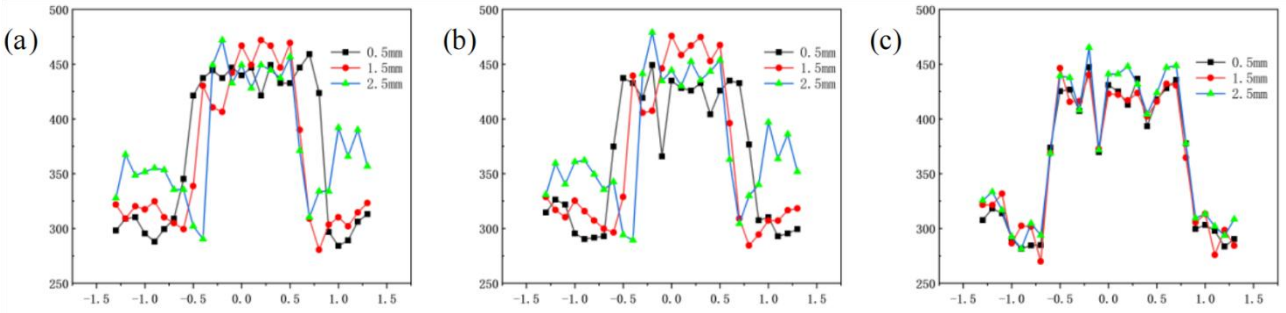

Figure 6. Power 4000W, welding speed 4m/min, defocus -4mm, shielding gas 20l/min surface grinding stateHardness of L-Bend welded joint. (a) Start of welding; (b) Welding middle; (c) End of welding

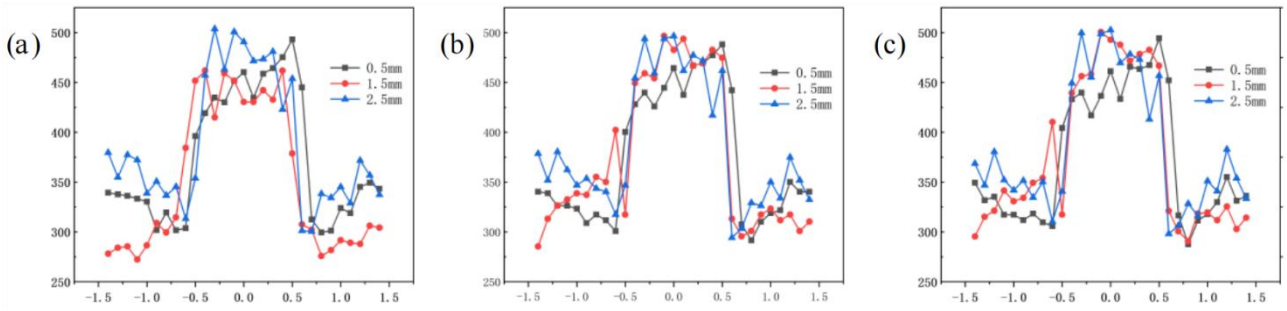

Figure 7. Original surface state L-Bend weld joint hardness (a) welding start; (b) Welding middle; (c) End of welding

Figure 6 shows the weld microhardness diagram at the beginning of welding (a), the middle of welding (b) and the end of welding (c). The softening zone of the welded joint in the oil coated state is 1.6mm, and the average hardness is 367.7hv. The hardness of the three surfaces has the same trend. However, the hardness of the welding starting surface is relatively low. It is speculated that at the beginning of welding, the laser will climb the slope, with high power, fast cooling speed and more martensite content. In the middle of welding, the laser intensity is stable, the cooling rate is moderate, the critical heat affected zone and heat affected zone are narrowed, and the hardness is gradually increasing. At the end of welding, the laser intensity is weak. It is speculated that the heat affected zone in this area is the narrowest, the content of ferrite retained austenite is the largest, and the hardness is the highest among the three surfaces. Figure 7 shows the hardness of welded joints in the original surface state.

4. CONCLUSION

The tensile strength of qp1500 base metal is 1496.28 MPa, and the elongation is 15.84%. The optimal parameters of laser tailor welding are laser power 4000W, welding speed 4m/min, defocus -2mm, argon 20L/min, tensile strength 1069.24 MPa and elongation 4.82%. The optimal laser L-Bend welding parameters are laser power 4000W, welding speed 4m/min, defocus -2mm, argon 20L/min, penetration depth 3.5mm, and fusion width 1.1mm.

The hardness of qp1500 welded joint at the beginning of welding, in the middle of welding and at the end of welding all have the same change trend. The hardness of the welding end surface is relatively high, and the hardness is gradually increasing. The hardness of the welding start surface is the lowest

REFERENCES

[1] De Moor, E., Lacroix, S., Clarke, A. et al. Effect of Retained Austenite Stabilized via Quench and Partitioning on the Strain Hardening

[2] Florian Vercruysse, Lisa Claeys, Tom Depover, Patricia Verleysen, Roumen H. Petrov, Kim Verbeken. The effect of Nb on the hydrogen embrittlement susceptibility of Q&P steel under static and dynamic loading. Materials Science and Engineering: A, Volume 852, 2022, 143652, ISSN 0921-5093.

[3] Xingchang Tang, Ganghu Cheng, Yajun Liu, Canglong Wang, Zhaocang Meng, Yinlong Wang, Yiwen Liu, Zhijian Zhang, Jiankang Huang, Xiaoquan Yu, Xueming Xu. Microstructure and properties evolution during annealing in low-carbon Nb containing steel with high strength and electrical conductivity: an experimental and theoretical study, Journal of Materials Research and Technology, Volume 27, 2023, Pages 3054-3066, ISSN 2238-7854.

[4] Mohrbacher, H.; Yang, J.-R.; Chen, Y.-W.; Rehrl, J.; Hebesberger, T. Metallurgical Effects of Niobium in Dual Phase Steel. Metals 2020, 10, 504.